Preliminary Analysis of the M_w 6.0 Wells, Nevada, Earthquake Sequence

by

Kenneth Smith[1], Jim Pechmann[2], Mark Meremonte[3] and Kristine Pankow[2]
[1]Nevada Seismological Laboratory, University of Nevada Reno
[2]University of Utah Seismograph Stations, Salt Lake City, UT
[3]U.S. Geological Survey, Golden, CO

2011

ABSTRACT

The February 2008 M_w 6.0 Wells, Nevada earthquake [Mo = 1.30 10^18 N-m; U.S. Geological Survey (USGS) CMT] sequence was a well recorded normal faulting event. The mainshock involved nearly pure normal displacement on a N40°E striking 55°SE dipping structure contributing to the development of Town Creek Flat basin, northeast of this small, rural Nevada community. The aftershock zone extends for approximately 20 km in an overall northeast-southwest trend with coseismic offset interpreted to be represented by an approximately circular region where the central part of the sequence is generally free of aftershock activity. The interpreted rupture radius of about 4 km implies a radial source with an estimated stress drop of 89 bars and average displacement of 86 cm. Early aftershock activity, including a number of the larger events of the sequence, was located southeast of the mainshock in the direction of the town of Wells. This suggests a component of rupture directivity to the southeast, which may have resulted in relatively higher ground motions in Wells. Fortunately, the EarthScope USArray network was operating in eastern Nevada at the time of the earthquake providing good epicentral control on the mainshock and early aftershock activity. Eventually, twenty-seven temporary portable stand-alone and telemetered seismographs were deployed in the region. High-quality HypoDD aftershock relocations image the mainshock fault plane at depth and details of the aftershock distribution. A review of the seismicity in Town Creek Flat basin since 2000 reveals that two M > 3 earthquakes (largest M 3.7 and felt in Wells) and a sequence of small events had occurred earlier near the location of the 2008 mainshock. This activity began on February 28, 2007, almost one year before the M_w 6.0 event. No surface faulting along a poorly defined range front was associated with the February 2008 Wells earthquake. We suggest that small basins such as Town Creek Flat, which accommodate regional deformation in association with large regional range-bounding normal faulting systems, could develop from repeated earthquakes with no direct surface expression.

INTRODUCTION

A M_w 6.0 normal-faulting earthquake occurred about 8 km northeast of the small rural northeast Nevada community of Wells on February 21, 2008 (Origin Time: 14:16:02.62 UTC; Latitude: 41.1656; Longitude: -114.8772; Depth: 8 km; figure 1). A number of unreinforced masonry structures in the old-town section dating to the early 20th century experienced significant damage; these building were uninhabited. There was also damage to some homes and businesses, including the local high school, but fortunately no one was seriously injured (see dePolo and others, this volume, for a discussion of ground motion effects from the Wells earthquake).

The 2008 Wells earthquake was the largest normal-faulting event in the Basin and Range Province since the 1993 M 6.1 Eureka Valley, California earthquake (Peltzer and Rosen, 1995). It took place in an area of relatively low seismic hazard (Peterson and others, 2008). Historical seismicity in the Basin and Range Province is primarily concentrated along its eastern and western margins and along an east to northeast trend of seismicity running through south central Nevada and southwestern Utah (Pancha and others, 2006; Rogers and others, 1991; Smith and Arabasz, 1991). Also, the Central Nevada Seismic Belt, a north-northeast trending zone of seismicity through west-central Nevada, has included 4 M about 7 surface-faulting earthquakes within the past 100 years (Bell and others, 2004; Wallace, 1984). The Wells event underscores the fact

that earthquakes can occur anywhere in the state of Nevada, and that areas of low seismic hazard are not without risk from damaging earthquake ground motions.
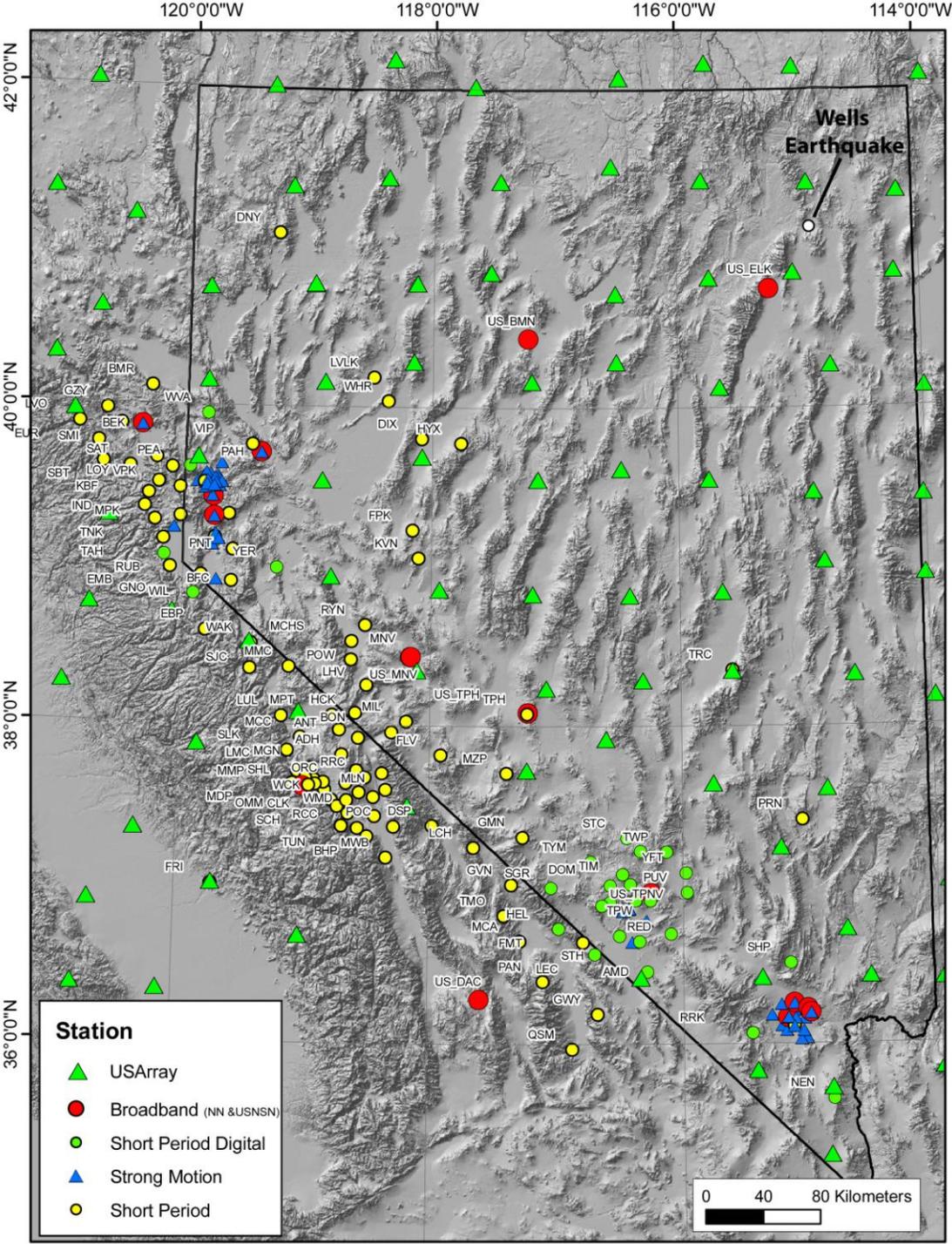

Figure 1. Regional monitoring stations in Nevada and eastern California including EarthScope USArray and USGS ANSS (USNSN) broadband stations. Also shown is the location of the Wells earthquake.

The earthquake occurred in Town Creek Flat (TCF) basin, a small northeast-elongated structure on the south end of the Snake Mountains in northern Clover Valley east of the East Humboldt Range (figure 2). The earthquake occurred directly east of a right step along the north-striking down-to-the-west Ruby Mountains and northern Snake Mountains frontal fault systems (see Henry and Colgan, and Ponce and others, this volume, for a detailed discussion of the regional geology and geophysics, respectively). No surface faulting has been identified for the Wells earthquake, and the event is not directly associated with previously mapped Quaternary faults, which is not an uncommon observation for moderate-sized earthquakes in the Basin and Range.
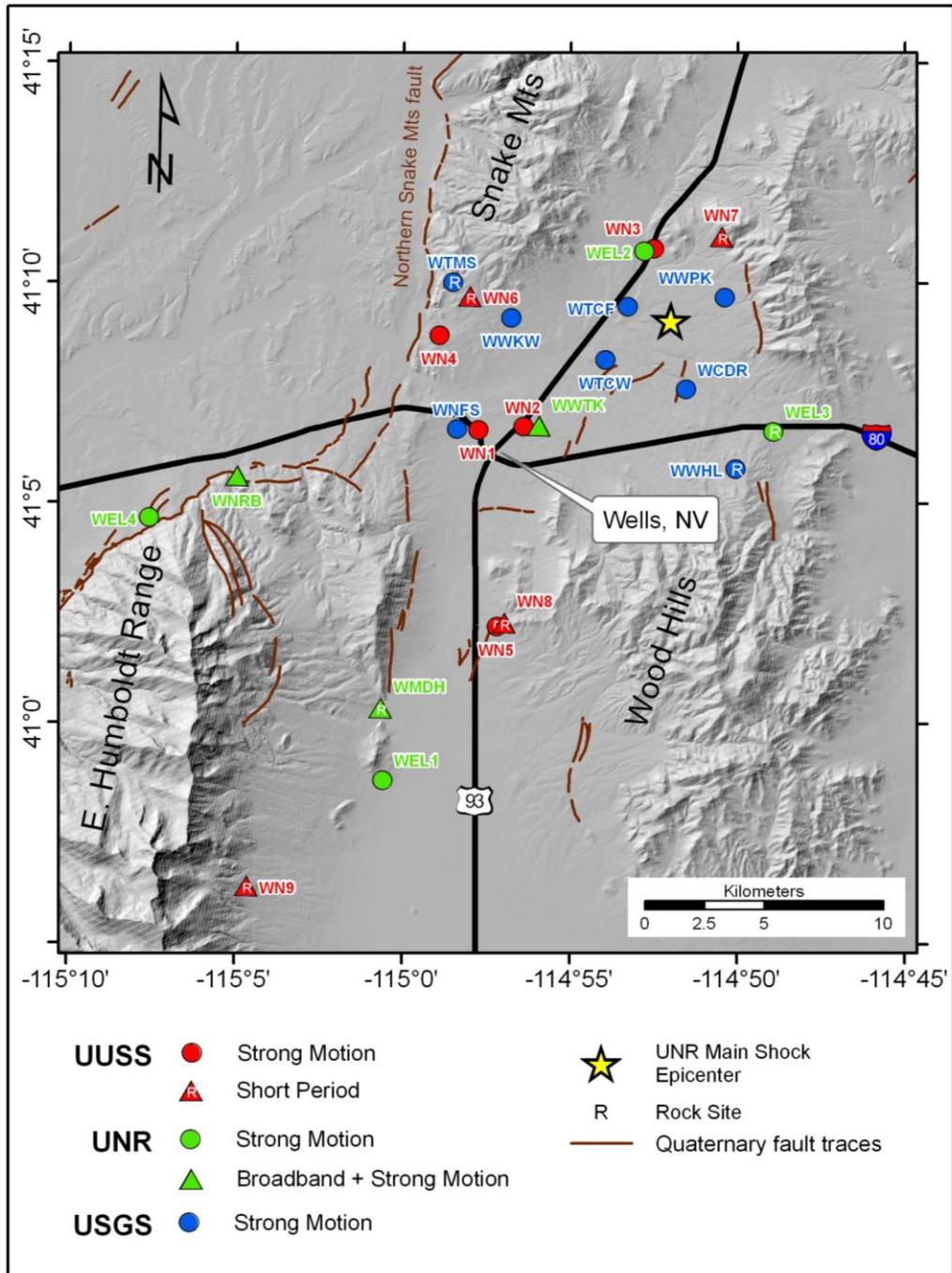
Figure 2. Map showing the distribution of temporary seismic stations deployed following the 2008 M_w 6.0 Wells earthquake (table 1). Three of the 27 stations are located southwest of the map area and are therefore not shown. Rock sites, which are indicated by an "R," are defined as sites for which the estimated bedrock depth is less than 5 m (Boore and Joyner, 1997). Town Creek Flat (TCF) basin is the broad lowland northeast of Wells that includes the mainshock and most of the portable deployment.

Table 1. Wells Area Temporary Station Deployment

Owner[1]	Name	Latitude (N)	Longitude (W)	Elevation (m)	Site Class[2]	Instrumentation (Digitizer, sensor(s))	Telemetry	Start Date (mm/dd, PST)	End Date (mm/dd, PST)
UU	WN1	41° 06.66	114° 57.76	1724	Soil	Kinemetrics Etna, internal Episensor	None	02/21	04/01
UU	WN2	41° 06.73	114° 56.41	1731	Soil	Kinemetrics Etna, internal Episensor	None	02/21	04/01
UU	WN3	41° 10.79	114° 52.52	1799	Soil	Kinemetrics Etna, internal Episensor	None	02/22	04/01
UU	WN4	41° 08.80	114° 58.93	1793	Soil	Kinemetrics Etna, internal Episensor	None	02/23	04/01
UU	WN5	41° 02.19	114° 57.19	1843	Rock	Kinemetrics Etna, internal Episensor	None	02/24	04/01
UU	WN6	41° 09.70	114° 58.01	1859	Rock	None, vertical Mark Products L-4	Analog	02/29	03/31
UU	WN7	41° 11.06	114° 50.48	2088	Rock	None, vertical Mark Products L-4	Analog	02/29	03/31
UU	WN8	41° 02.29	114° 56.96	1878	Rock	None, 3-comp. set of Mark Products L-4's	Analog	02/29	03/31
UU	WN9	40° 56.30	115° 04.63	2161	Rock	None, vertical Mark Products L-4	Analog	02/29	03/31
UNR	WEL1	40° 58.70	115° 00.60	1784	Soil	Kinemetrics Etna, internal Episensor	None	02/22	
UNR	WEL2	41° 10.73	114° 52.82	1773	Soil	Kinemetrics K2, internal Episensor	None	02/22	
UNR	WEL3	41° 06.63	114° 48.94	1912	Rock	Kinemetrics K2, internal Episensor	None	02/22	
UNR	WEL4	41° 04.66	115° 07.58	1797	Soil	Kinemetrics Etna, internal Episensor	None	02/22	
UNR	WJGS	40° 28.55	115° 35.27	1924	Soil	REF TEK 130, Trillium 40, external Episensor	None	03/08	04/30
UNR	WLAM	40° 41.38	115° 28.34	1960	Rock	REF TEK 130, Trillium 40, external Episensor	Digital	04/02	04/30
UNR	WMDH	41° 00.34	115° 00.64	1797	Rock	REF TEK 130, Trillium 40, external Episensor	None	03/10	04/30
UNR	WNRB	41° 05.60	115° 04.94	1808	Soil	REF TEK 130, Trillium 40, external Episensor	Digital	04/03	04/30
UNR	WSCR	40° 51.92	115° 15.27	1817	Rock	REF TEK 130, Trillium 40, external Episensor	Digital	04/03	04/30
UNR	WWTK	41° 06.76	114° 55.93	1738	Soil	REF TEK 130, Trillium 40, external Episensor	Digital	03/10	04/30
USGS	WCDR	41° 07.59	114° 51.56	1809	Soil	REF TEK 130, external MEMS	Digital (after 2/28)	02/23	05/19
USGS	WNFS	41° 06.67	114° 58.40	1723	Soil	REF TEK 130, external MEMS	Digital (after 2/28)	02/23	Still operating
USGS	WTCF	41° 09.46	114° 53.31	1766	Soil	REF TEK 130, external MEMS	Digital (after 2/28)	02/25	05/20
USGS	WTCW	41° 08.26	114° 53.97	1763	Soil	REF TEK 130, external MEMS	Digital (after 2/28)	02/23	05/19
USGS	WTMS	41° 10.01	114° 58.52	1824	Rock	REF TEK 130, external MEMS	Digital (after 2/28)	02/23	Still operating
USGS	WWHL	41° 05.78	114° 50.07	1982	Rock	REF TEK 130, external MEMS	Digital (after 2/28)	02/24	05/19
USGS	WWKW	41° 09.20	114° 56.78	1781	Soil	REF TEK 130, external MEMS	Digital (after 2/28)	02/23	05/19
USGS	WWPK	41° 09.67	114° 50.41	1887	Soil	REF TEK 130, external MEMS	Digital (after 2/28)	02/25	05/20

[1]UU, University of Utah; UNR, University of Nevada, Reno; USGS, U.S. Geological Survey, Golden, Colorado
[2]Following Boore and Joyner (1997), we classify sites as rock sites if the estimated soil depth is less than 5 m.

Although the Nevada historical earthquake catalog includes a record of seismicity near Wells, station coverage and location quality have been poor in the northeastern part of the state, making it difficult to assess the historical record. At the time of the earthquake, the only permanent seismic station operating in the region was the U.S. Geological Survey (USGS) Advanced National Seismic System (ANSS; see http://www.anss.org) station ELK east of Elko, Nevada (figure 1). Fortunately, the EarthScope USArray Transportable network (see http://www.earthscope.org and Busby, 2007) was operating in eastern Nevada (figure 1) at the time of the event and provided unique controls on the mainshock and early aftershock locations (figure 1). USArray continued to provide regional coverage until its removal from northeastern Nevada in the fall of 2008. The best control on aftershock locations in the Wells area was provided by 27 temporary stations (see following section).

Recent regional normal faulting events prior to the 2008 Wells earthquake include the 1999 M 5.6 Scottys Junction, Nevada, the 1995 M 4.5 Bordertown, Nevada (Ichinose and others, 1996), the 1993 M 6.1 Eureka Valley, California (Peltzer and Rosen, 1995), the 1992 M 5.6 Little Skull Mountain, Nevada (Meremonte and others, 1995; Smith et al, 2001), and 1992 M 5.8 St. George, Utah (Pechmann and others, 1994; Christenson, 1995) earthquakes. These more recent normal faulting events predated modern field communications capabilities, and relied on analog telemetry and/or near-source, stand-alone, portable instruments to supplement regional networks for high-quality aftershock locations. This preliminary analysis of the Wells aftershock sequence was greatly improved by the implementation of a wireless IP (Internet Protocol) communications network with real-time digital telemetry to temporary portable instruments (see figure 2 and table 1; instruments labeled USGS "Strong Motion" are telemetered). The telemetry system enabled real-time notifications, simplified data management, improved data quality, provided real-time data to national data centers, and ultimately reduced field maintenance costs. Considering the volume of data collected in the sequence, especially on-scale ground motion in the early aftershock period, only a preliminary analysis is provided here. This unprecedented near-source data set for a normal faulting sequence is evidence of the effectiveness of the USGS ANSS cooperative program. Field efforts and data management were coordinated among University of Utah (UU), USGS, and Nevada Seismological Laboratory (NSL) staff.

TEMPORARY STATION DEPLOYMENT

Following the earthquake, the NSL, UU, and the USGS eventually deployed a total of 27 temporary stations in the Wells area. The equipment at six of the stations installed by NSL was on temporary loan from National Science Foundation Rapid Array Mobilization Program (RAMP) through the Passcal Instrument Center in Socorro, New Mexico (see: http://www.passcal.nmt.edu). Figure 2 shows the locations of stations in the temporary network located directly in the Wells area. The University of Utah installed the initial portable instruments on the day of the earthquake (WN1 and WN2, table 1). By the end of the first day, UU and UNR had installed seven locally recorded digital instruments. Within three days of the event, UU and USGS had deployed 8 additional near-source, locally recorded digital instruments, and by February 29th a total of 21 digital recorders were operational. The RAMP stations were installed between March 8 and April 3 to collect data at more regional distances along the Ruby Mountains and to monitor for potential triggered seismicity along the Ruby Mountains range front.

Twenty-three of the twenty-seven temporary stations were equipped with 3-component Kinemetrics Episensors or RefTek 131A-2/3 MEMS accelerometers. Although accelerometers have traditionally been used primarily for recording strong ground motions from large earthquakes, modern accelerometers with high dynamic range dataloggers are sensitive to low magnitude events at distances of up to about 100 km (Clinton and Heaton, 2002; Pankow and others, 2007). Also, the use of accelerometers ensures that the largest earthquakes remain on-scale and those most important events for ground motion and sources studies remain on-scale. The six RAMP stations were configured with Nanometrics 3-component Trillium 40 broadband seismometers in addition to 3-component accelerometers. The sensors at four of the UU stations were vertical- or 3-component Mark Products L-4 short period (1 Hz) seismometers.

Ultimately data from sixteen of the twenty-seven temporary stations were telemetered in real time to recording centers at UNR or the UU. Continuous analog data from the four UU short-period stations were telemetered to the UU, where they were digitized, recorded, and transmitted to UNR, in real time, via an Earthworm export. (Earthworm is a suite of real-time data processing applications developed by the U.S. Geological Survey; see: http://folkworm.ceri.memphis.edu/ew-doc). Four of the six NSL RAMP stations telemetered continuous digital data to UNR using cellular modems. All eight of the USGS strong-motion stations sent continuous digital data to UNR using the communications network described below. Telemetry for the USGS stations did not begin until 3 to 5 days after station installation; data were recorded locally prior to establishing real-time communications. The remaining stations recorded continuous digital data on site (table 1).

Digital telemetry of the USGS temporary stations to UNR was established by February 29th using a point-to-multipoint IP communications network within the TCF basin. This network employed Motorola 900 MHz Canopy SM (Subscriber Module) radios with line-of-sight to a 900 MHz Canopy AP (Access Point) radio installed at the Nevada Department of Information Technology's (DoIT) Turner Station microwave site outside of Wells (figure 3). DoIT provided a T1 circuit and UNR installed a Cisco 2811 router with the AP in the DoIT facility at Turner Station. The data were transmitted

through the DoIT microwave system to a mountaintop site outside of Las Vegas where they were integrated with NSL's southern Nevada communications systems. A salient feature of the Wells portable instrument telemetry system is that all IP devices, including radios, routers and dataloggers, were on the NSL private network and directly managed from NSL. This setup avoided problems encountered in interacting with local ISPs or in addressing firewalls or other third party networking idiosyncrasies. The real-time data were forwarded to the IRIS Data Management Center (IRIS DMC) in Seattle, Washington, and are publicly available.
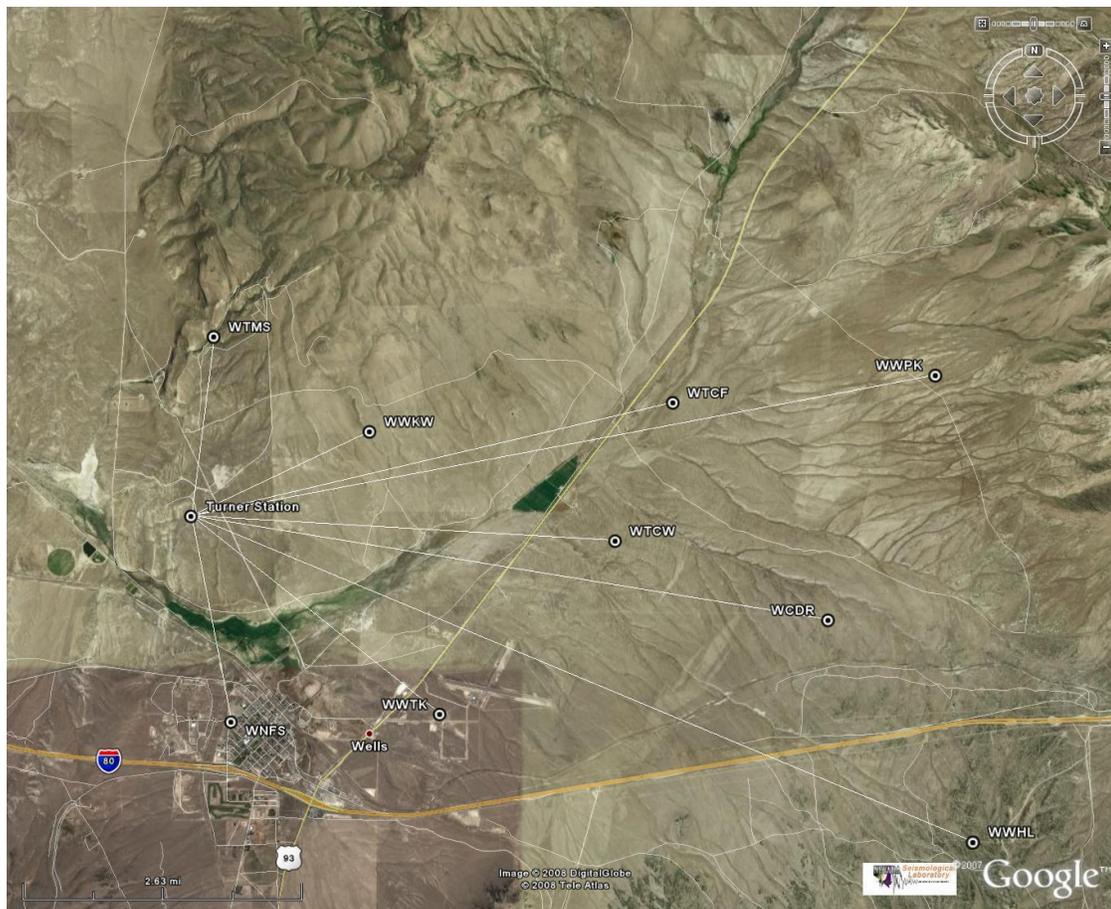
Figure 3. Map of telemetry paths for USGS RT130 instruments to DoIT relay Turner Station (map using software application Google Earth http://earth.google.com/).

The majority of the temporary stations were installed at free-field sites, and the remainder in small, one-story buildings in Wells. Winter weather and snow cover greatly impeded travel off paved roads and hindered the search for suitable recording sites, especially hard rock sites and those at higher elevations. Many of the stations were installed and maintained using Sno-Cats and snowmobiles provided by county and state government agencies and local businesses. However, even with these types of vehicles it was not possible to reach some of the planned recording sites. The original station siting plans were revised significantly during the course of the field operations to take into account the practical realities of the field conditions. These revisions, in combination with communications issues, led to some redundancy in the station locations. A further complicating factor was the migration of the aftershock zone to the north as the sequence evolved; access to northern locations was difficult. The final distribution of temporary stations was reasonably good, but not entirely optimal for monitoring the final geographic extent of the aftershock distribution (figure 2).

The four UU short-period analog telemetry stations were installed primarily for use in aftershock locations. These stations were located at rock sites in the hills surrounding the aftershock zone (WN6, WN7, and WN8) and at a radio relay point 20 km south-southwest of Wells (WN9; figure 2). The five UU and four UNR "strong motion" accelerograph stations (WN1-WN5 and WEL1-WEL4; figure 2) were installed at both soil and rock sites with two main applications in mind: aftershock locations and the near-field recording of potential strong ground motions and to capture potentially larger events on nearby faults that may have been triggered by the M_W 6.0 event. The eight USGS strong-motion stations were deployed along two profiles in order to collect data for studying the variation of ground motion amplification across TCF basin

(figure 2). The first profile extended southeastward across this valley from the southern end of the Snake Mountains to the northern end of the Wood Hills (stations WTMS, WWKW, WTCW, WCDR, and WWHL). The second profile extended northeastward from Wells (stations WNFS, WTCW, WTCF, and WWPK) and was augmented by UU and UNR stations. Four of the six UNR RAMP stations—WNRB, WSCR, WLAM, and WJGS (table 1; the latter three are not on figure 2)— formed an 80-km-long southwest-trending line along the west side of the East Humboldt Range and the Ruby Mountains. The purposes of this profile were to collect data for crustal structure studies using Wells aftershocks as sources and to monitor for potentially triggered seismicity along the Ruby Mountains range front.

OTHER DATA

As noted above, the primary data source for the mainshock and early aftershock locations and ground motions was the EarthScope USArray "TA" network (figure 1). Data from TA stations are received directly from the USArray Array Network Facility at U.C. San Diego via an Antelope data transfer (Antelope is a product of Boulder Real Time System, Boulder, CO). The only permanent station in the region is ANSS broadband ELK on the east side of the Ruby Mountains east of Elko, Nevada (figure 1). Station ELK is operated by the U.S. Geological Survey; all ANSS regional broadband data are received in real time at NSL via an Earthworm import.

EVENT LOCATIONS

For the foreshock period, mainshock, and initial aftershocks, TA network and ELK phase arrival times provide good epicentral control but large distances and limited constraints on the regional velocity structure in eastern Nevada result in poor depth control. With the portable deployment, near-source phase data supplemented by TA stations provide very good hypocentral depth estimates. At the time of this report, integration of the data from all non-telemetered temporary stations is not complete. The data from the telemetered portable stations and the TA network provide a consistent set of arrival times for the preliminary relocations reported here.

The Wells sequence was relocated with application HypoDD (Waldhauser and Ellsworth, 2000) from phase arrival times and by applying the velocity model shown in table 2. This is a hybrid model that includes a mid- to lower-crustal velocity structure used in the Salt Lake City area (Pechmann, personal communication) and a shallow velocity structure consistent with other areas of Nevada. Due to near-source S-arrival times from multiple stations there is little change in hypocentral depths for high-quality locations from reasonable changes in the upper crustal velocity structure. The model with a 1-km thick surface layer with P-wave speed of 4.0 km/s (table 2) reduced the number of unusually shallow (< 2 km) event locations and results in a "best set" of event locations described here. All preliminary locations and phase arrival times were computed within the Antelope data management system and are archived in the DataScope relational database at NSL (Quinlin, 1995). Phase data were recovered from the DataScope database and preprocessed with application PH2DT prior to relocation with HypoDD. HypoDD establishes a set of relative event locations based on inter-event phase arrival and waveform cross-correlation times, when available. Event locations are determined relative to the average station elevation, which is 1.82 km above sea level for the near-source portable instruments deployed in the TCF basin (figure 4).

Table 2. Velocity Model for Wells Relocations

Depth of Top of Layer (km)	P-Wave Velocity (km/s)
0.0	4.0
1.0	5.5
3.0	5.8
18.0	6.5
25.0	7.5
42.0	7.9
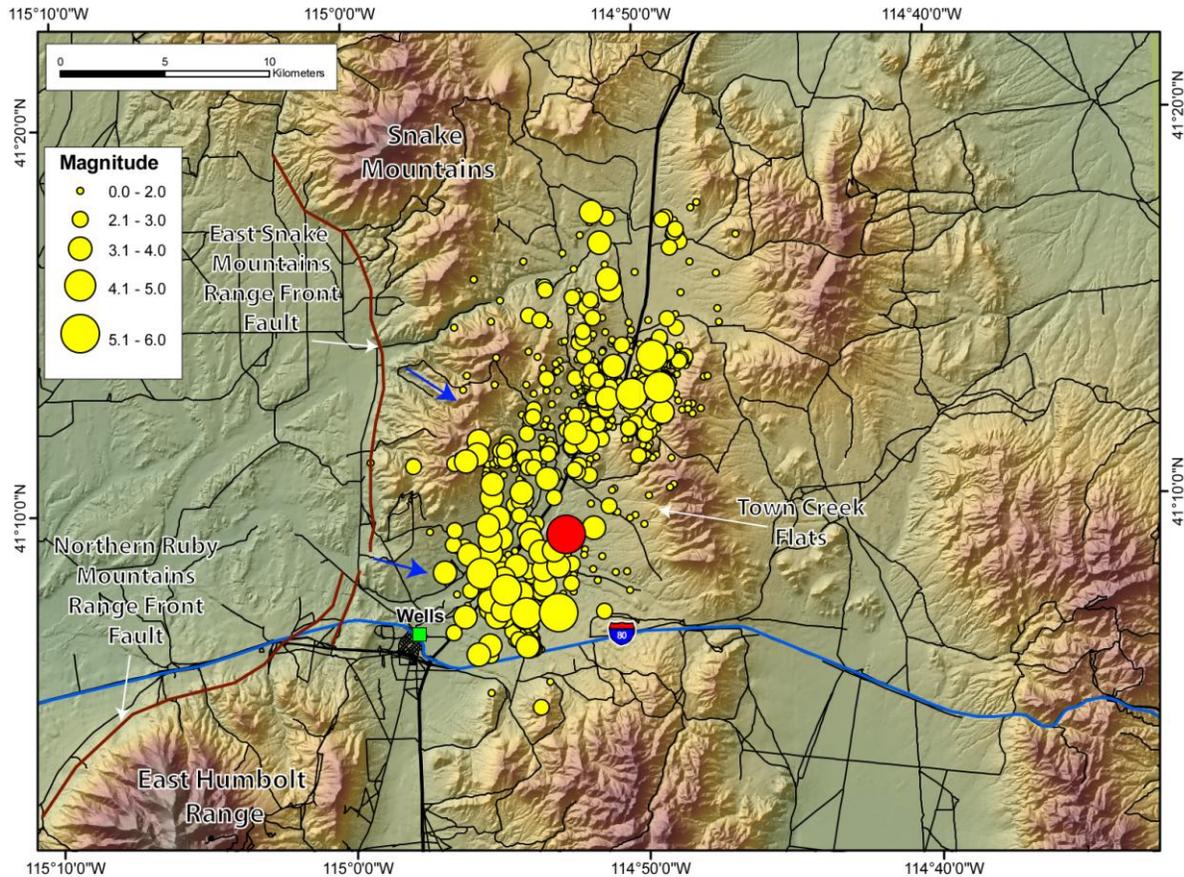
Figure 4. HypoDD relocations of the Wells sequence. Labeled are the physiographic features referenced in the text and the Ruby Mountains and East Snake Mountains range frontal fault systems. Blue arrows are for perspective views, figures 11 (view toward the SE) and 12 (view ESE).

WELLS MAINSHOCK

Mainshock moment tensor solutions developed from regional and global data are summarized in table 3. All moment tensor solutions for the mainshock are consistent with a north-northeast-striking normal fault dipping either west-northwest or east-southeast. The centroid depths range from 7 to 14 km; however, constraining the mainshock hypocentral depth from body wave arrival time data is difficult due to limited station coverage (no near-source stations) and lack of knowledge about the velocity structure in eastern Nevada. The closest station was at a distance of 36 km with most (TA) at distances greater than 100 km. Fortunately, USArray stations and station ELK (figure 1) provide good epicentral control, and the extent of faulting during the main event is established by high-quality aftershock locations developed subsequently with data from near-source instruments. We estimate the mainshock depth to be 8 km based on high-quality aftershock locations described below.

Table 3. M_W 6.0 Moment Tensor Solutions by Organization

Agency	Mo (N-m)	Strike-Dip-Rake	Depth (km)	T-axis (strike-plunge)
USGS CMT	1.30*10^18	9 58 -114	10.0	116 9
Harvard CMT	1.4*10^18	30 40 -86	13.5	297 6
USGS Body Wave	6.8*10^17	19 33 -96	7.0	293 12
SLU[*]	8.32*10^17	25 40 -90	11.0	295 5
Dreger and others, 2008	7.86-8.89*10^17	34 40 -83	7-10	

[*]SLU - St. Louis University

134

PRIOR SEISMICITY IN TCF AND WELLS FORESHOCK ACTIVITY

We computed HypoDD relocations for prior seismicity in the Wells, 2000 through the February 21, 2008, mainshock (figure 5). Prior to USArray operations in eastern Nevada (spring of 2006), it is difficult if not impossible, to assess the earthquake activity in the TCF basin area (see figure 1; eastern Nevada seismograph stations). Based on USArray data, the first earthquake activity observed in the vicinity of the eventual mainshock began February 28, 2007 with M 3.7 (Origin Time: 11:47:41.32 UTC) and M 3.1 (Origin Time: 14:46:10.23) earthquakes that were both felt in Wells. Based on historical network coverage, we cannot effectively evaluate the pre-USArray seismcity in the TCF or in the region in general. Altogether, 65 locatable earthquakes, including some immediate foreshocks, occurred in the Wells area within the year prior to the 2008 mainshock (figure 6). Figure 5 shows a set of HypoDD relocations of this activity and figure 6 shows its temporal progression from the February 2007 M 3.7 earthquake through the M_w 6.0 main event. Figure 6 shows that three events were located in the Wells area in the eight days prior to the mainshock. HypoDD relocations significantly improve foreshock locations and clearly define the clustering of prior seismicity and immediate foreshock activity in the mainshock area as compared to the scatter in initial catalog locations (initial catalog locations not shown). Because phase arrivals for the prior activity have not been reviewed for all located events, some of the locations may be in question. However, it is clear that most of this activity, including both M > 3 events, occurred near the 2008 mainshock (figure 5). Further resolution of foreshock depths has not been attempted. Review of the continuous waveform data at USArray station NA12 (36 km to the south) shows no activity in the Wells area on the day prior to the 2008 M_w 6.0 earthquake. In retrospect, and a potential lesson from Wells is that unusual felt events and continuing activity in rural communities of low seismic hazard could focus monitoring efforts and motivate hazard mitigation efforts.
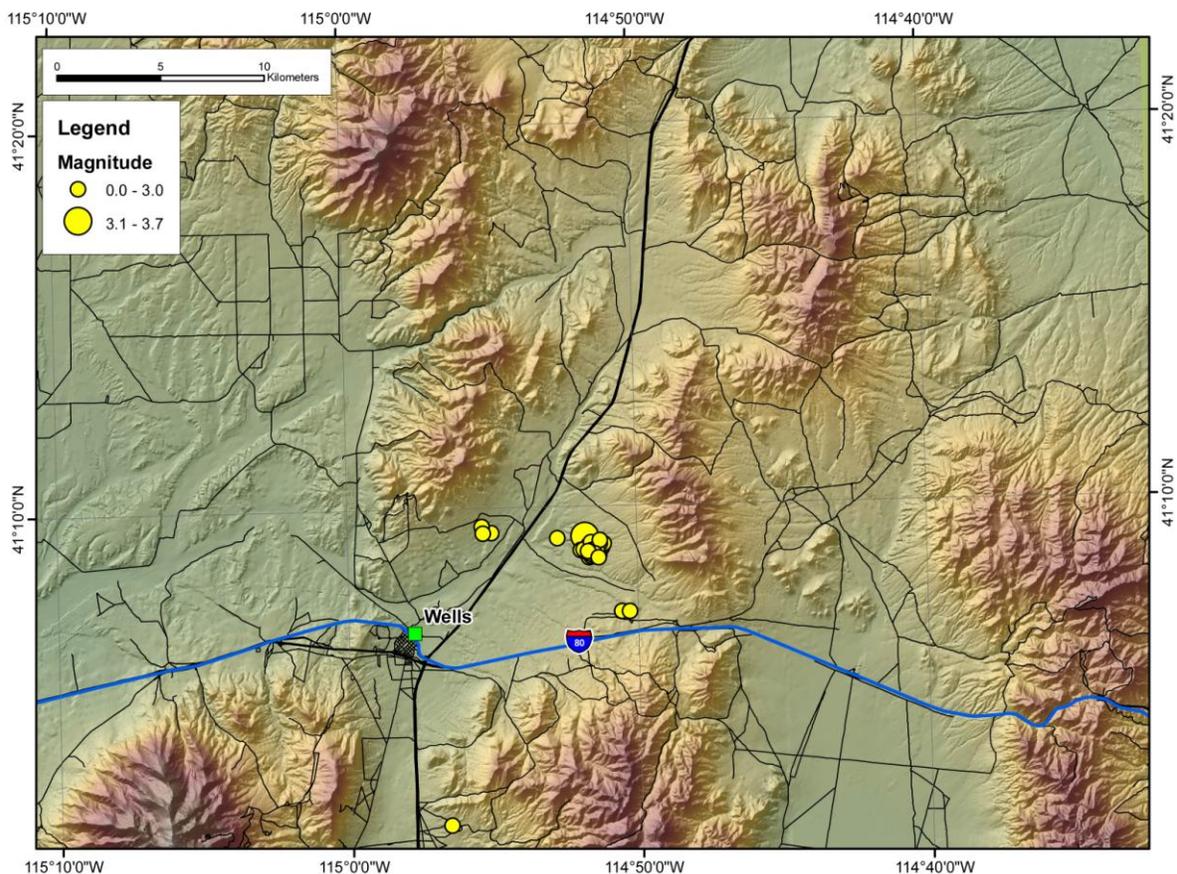

Figure 5. HypoDD relocations of activity recorded in the TCF area from January 2000 through February 21, 2008. All events shown occurred before February 28, 2007.

135
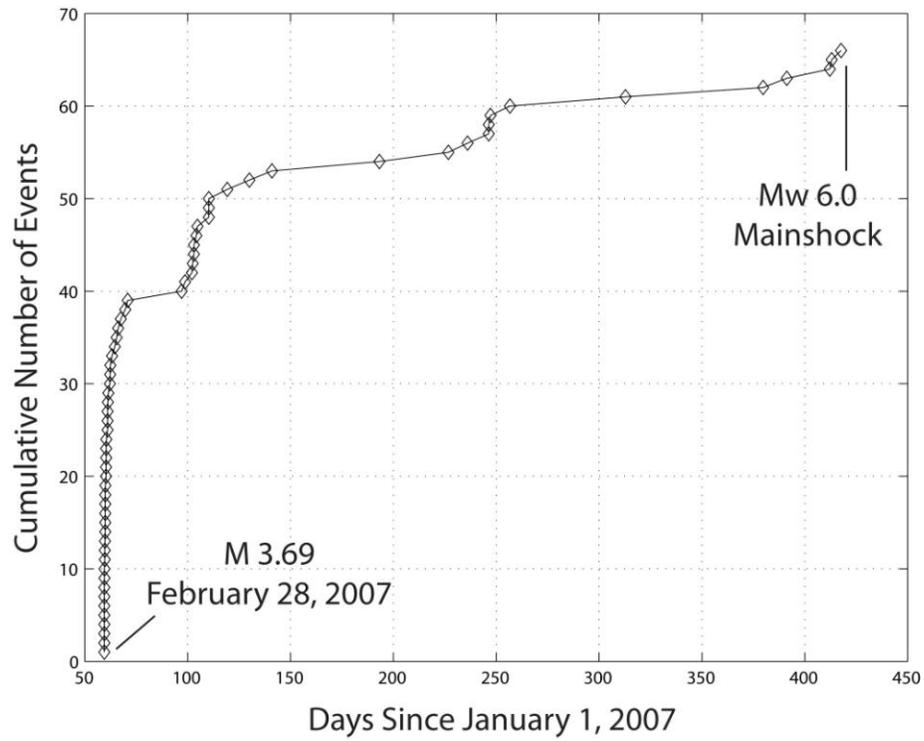
Figure 6. Time sequence of cumulative number of located events preceding the M_W 6.0 Wells mainshock on February 21, 2008.
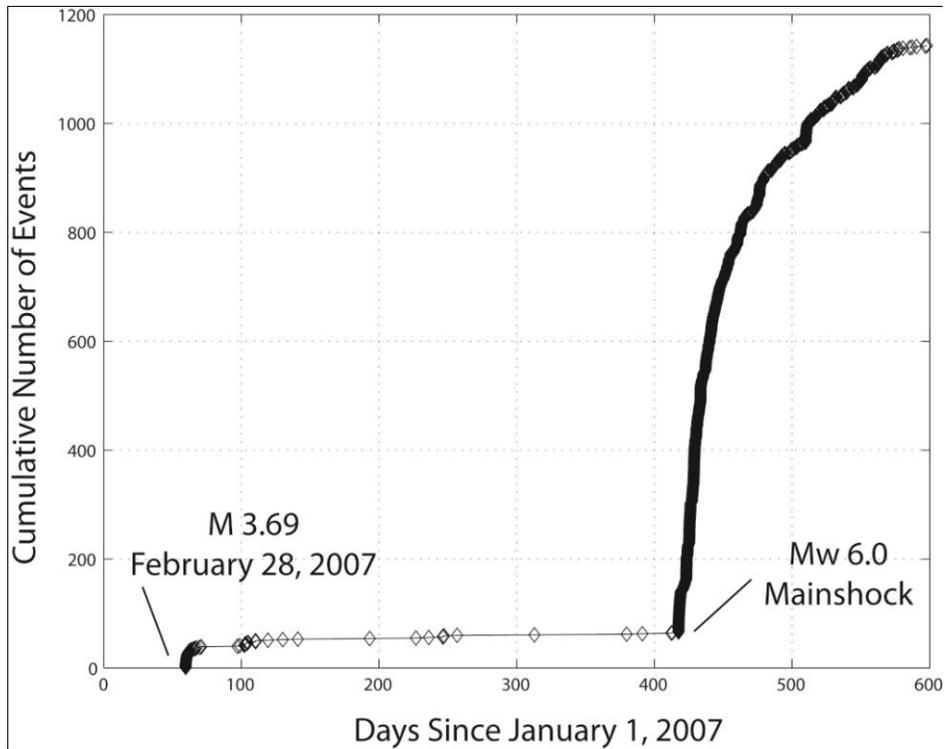
Figure 7. Time sequence of cumulative number of events through October 18, 2008.

136

AFTERSHOCK RELOCATIONS AND PRIMARY FAULTING

Figure 4 shows a set of HypoDD relocations for the Wells earthquake sequence through October 16, 2008, and figure 7 shows the temporal progression of the foreshock-mainshock-aftershock sequence through mid-October 2008. Figure 8 shows the raw catalog locations for the initial 40 hours of the sequence, which included many of the largest aftershocks. HypoDD relocations were not performed because these events were located only using USArray and ANSS stations ELK and BMN (figure 1), limiting depth control. Figure 9 shows event locations determined from near-source real-time telemetered data only; these are the best event locations. Table 4 lists aftershock moment tensor solutions computed by St. Louis University (see: http://www.eas.slu.edu/Earthquake_Center/MECH.NA/), and table 5 lists all Wells earthquakes larger than M 3.5 through mid-October 2008 (table 5, UNR local magnitudes unless noted; locations are not included since these may change with further analysis). The ten regional mechanisms (table 4) show primary normal faulting, except for an M_w 4.1 strike-slip event at 07:59 UTC February 27th and an M_w 4.1 oblique-slip event at 13:16 UTC April 1st, 2008 (table 4). All mechanisms show a northwest-southeast T-axis orientation with one exception (M_w 3.8, 2008/04/22, 20:04 UTC, shows an east-west T-axis). It is not unusual to see some variability in focal mechanisms with respect to the mainshock mechanism (principal moment release) within an aftershock zone.
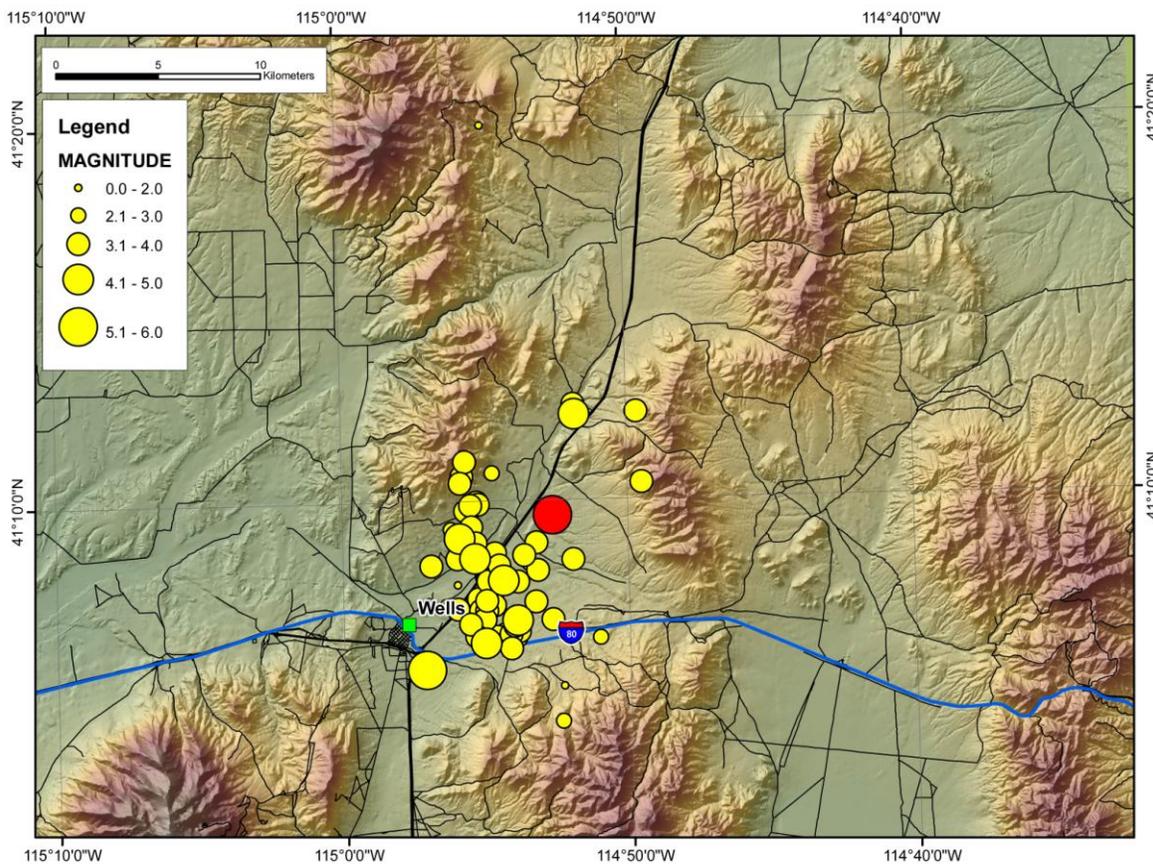
Figure 8. NSL raw catalog locations for Wells area earthquakes, February 21 and 22, 2008 (not relocated). The mainshock is the red symbol. No portable instrument data are used to develop these locations.
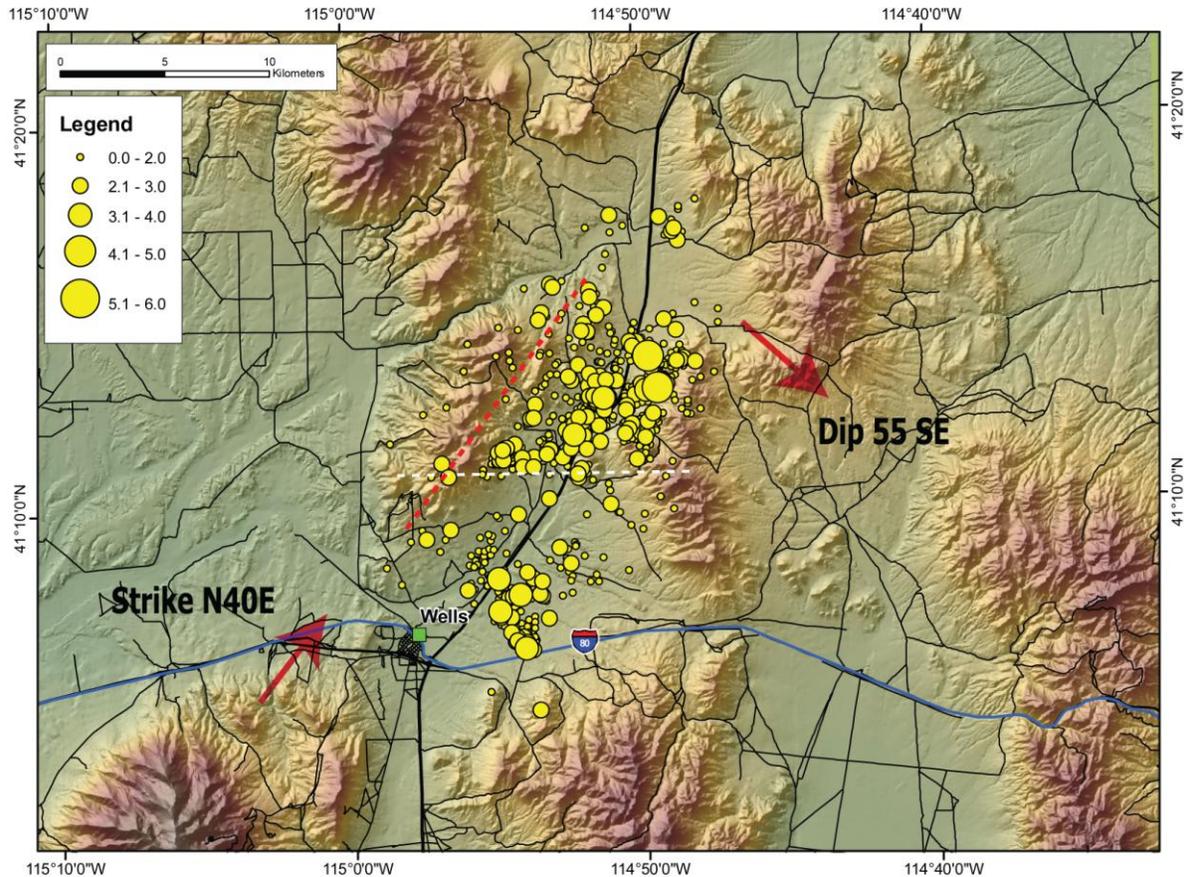
Figure 9. HypoDD relocations for earthquakes recorded following installation of real-time portable instruments on February 29; event relocations through October 18, 2008. The red dashed line is the interpreted surface projection of the Wells mainshock fault plane and the white dashed line is the interpreted intersection of the mainshock fault plane with a potential structure defined by aeromagnetic data and discussed in Ponce and others (this volume).

Table 4. Wells events with Moment Tensor Solutions (M_W)

Date	Time (UTC)	M_w	Strike-Dip-Rake
2008/02/21	14:16:05	5.8[1]	205 50 -90
2008/02/21	16:20:02	3.9	354 48 -129
2008/02/21	23:57:52	4.6	19 68 -118
2008/02/22	01:50:06	3.7	5 45 -126
2008/02/22	23:27:46	4.3	38 50 -94
2008/02/27	07:59:39	4.1[2]	90 85 10
2008/02/28	15:10:39	4.0	22 61 -118
2008/03/15	16:22:35	3.6	45 45 -95
2008/04/01	13:16:17	4.1[3]	85 50 -15
2008/04/22	20:04:09	3.8	45 30 -55

[1]Mainshock M_W 5.8 reported by SLU and solutions with strike-slip [2] or oblique [3] faulting mechanisms. M_Ws reported by SLU (Bob Herrmann) regional moment tensor solutions for North American earthquakes. http://www.eas.slu.edu/Earthquake_Center/MECH.NA.

The mainshock epicenter is located within a zone that is generally free of aftershocks within the central part of the sequence (figure 4, 8 and 9). This is often observed for moderate-sized Basin and Range earthquakes and has been interpreted to represent the extent of coseismic displacement and the rupture area of primary faulting (e.g., Smith and

others, 2001; Priestley and others, 1986; Smith and Priestley, 2000). Aftershock activity within the initial 40 hours of the mainshock (figure 8) is concentrated in the direction of the city of Wells suggesting a component of rupture directivity to the southwest. This is consistent with slip models with areas of greater energy release southwest of the mainshock hypocenter, even within an overall bi-lateral rupture process (Dreger and others, this volume). We estimate the hypocentral depth of the mainshock from the projections of the mainshock epicenter with the imaged fault plane at depth; mainshock depth control is limited by the lack of near-source stations. The mainshock hypocenter would not be expected to be located off the main rupture surface.

Table 5. Wells events larger than M 3.5 (UNR Local Magnitude) through October 18, 2008

DATE	Time (UTC)	M
2007/02/28	11:47:41	3.7
2008/02/21	**14:16:02**	**6.0**[*]
2008/02/21	14:20:51	4.7
2008/02/21	14:34:43	5.1
2008/02/21	14:46:31	3.6
2008/02/21	15:34:25	4.1
2008/02/21	16:20:02	4.3
2008/02/21	16:25:49	3.7
2008/02/21	16:39:29	3.8
2008/02/21	17:01:46	3.5
2008/02/21	19:37:08	3.6
2008/02/21	19:53:49	3.6
2008/02/21	19:57:19	3.8
2008/02/21	20:04:58	3.8
2008/02/21	22:47:28	3.6
2008/02/21	23:57:51	4.8
2008/02/22	01:50:05	4.3
2008/02/22	05:07:22	3.5
2008/02/22	11:05:29	3.6
2008/02/22	11:17:24	3.5
2008/02/22	15:30:22	3.7
2008/02/22	17:10:20	3.5
2008/02/22	17:31:45	3.5
2008/02/22	18:30:19	3.5
2008/02/22	19:22:30	3.7
2008/02/22	23:24:03	3.7
2008/02/22	23:27:45	4.7
2008/02/26	02:22:23	3.6
2008/02/27	07:59:38	4.6
2008/02/28	15:10:37	4.0
2008/03/03	22:45:02	3.5
2008/03/15	16:22:33	3.8
2008/04/01	13:16:17	4.7
2008/04/22	20:40:09	4.3

[*]All magnitudes UNR NSL local magnitude except for the M_w 6.0 mainshock.

Imaging of the fault plane at depth and interpretation of the extent of rupture are based on HypoDD relocations developed from the telemetered portable instrument deployment period only (figures 9, 10, 11, 12 and 13). Near-source P- and S-arrival times from the portable array provide the best control on aftershock locations, and therefore these locations are used to interpret the features of Wells faulting. Also, since these data were received in real-time they are already integrated with other regional network and TA data in local databases. Figure 9 is a map view of relocated hypocenters and figure 10 is a cross-section view from the SW in the N40E direction (along strike of the mainshock fault plane). No surface displacement has been recognized from the Wells event; faulting was most likely confined to the subsurface. An estimate of the surface projection of the imaged fault plane daylights within Snake Mountains range block to the north (figure 9). The surface projection of the mainshock fault plane is not associated with a mapped fault along the southeast Snake Mountains.

Most aftershock hypocenters shown in figures 9 and 10 define a plane striking approximately N40°E and dipping 55° SE. The cross-section (figure 10) may suggest a listric geometry; however, this results from the shallow apparent dip of events at the southwestern extent of the aftershock zone and is not characteristic of the entire length of the aftershock zone at depth. Figures 11 and 12 are views down-dip along the mainshock fault plane at 55° and 42° to the SE and ESE, respectively, illustrating both the dip of the primary section of the mainshock fault plane (figure 11) and the shallow dip of the narrow aftershock alignment at the southwestern extent of the sequence (figure 12). An alternative interpretation to a listric component of slip at the southwest end of the mainshock fault plane is that this activity represents triggered seismicity on a north-south striking east-dipping structure along the east side of the East Humboldt Range (see electronic supplemental information for 3D image of the aftershock sequence). Compared to the northeast edge of the aftershock zone, the southwestern edge terminates abruptly; suggesting that the mainshock rupture intersects another structure at depth. This interpretation is consistent with the intersection of the Wells mainshock fault plane with a down-to-the-east structure along the east side of the East Humboldt Range in northern Clover Valley. Also the Wells fault plane could represent a northeast extension of this structure (see Henry and Colgan, this volume). The southward decrease in the number of aftershocks within this central section slightly south of the mainshock suggests a potential high-angle structure that intersects the central section of the mainshock fault plane (figures 9 and 12; illustrated by dashed white line in figure 9). This feature in the aftershock distribution is generally consistent with the location of an east-west striking structure interpreted from aeromagnetic data (Ponce and others, this volume) that intersects the mainshock fault plane.

The coseismic displacement, interpreted to be the area that is generally free of aftershocks in the central part of the sequence, is roughly circular with an estimated radius of approximately 4 km, suggesting a radial rupture. The depth distribution of relocated events also indicates a zone in the mainshock depth range where there are fewer aftershocks (figure 13). Aftershocks are concentrated in the 4-6 and 8-10 km depth ranges. Given an estimated rupture radius, r, and seismic moment Mo, the static stress drop and average displacement can be estimated. The static stress drop, σ, is (Brune 1970),

$\sigma = \dfrac{7}{16}\dfrac{Mo}{r^3}$. The average displacement, u, is, $u = \dfrac{Mo}{\mu A}$, where, the rigidity, μ, is an assumed $3*10^{11}$ dyne/cm^2 and the seismic moment, Mo, is $1.30*10^{18}$ N-m (table 3; USGS CMT). This model results in a static stress drop of 89 bars and average displacement of 86 cm. These estimates are very consistent with and similar to regional slip inversion results of Dreger and others, (2008) and Mendoza and others, (2008).
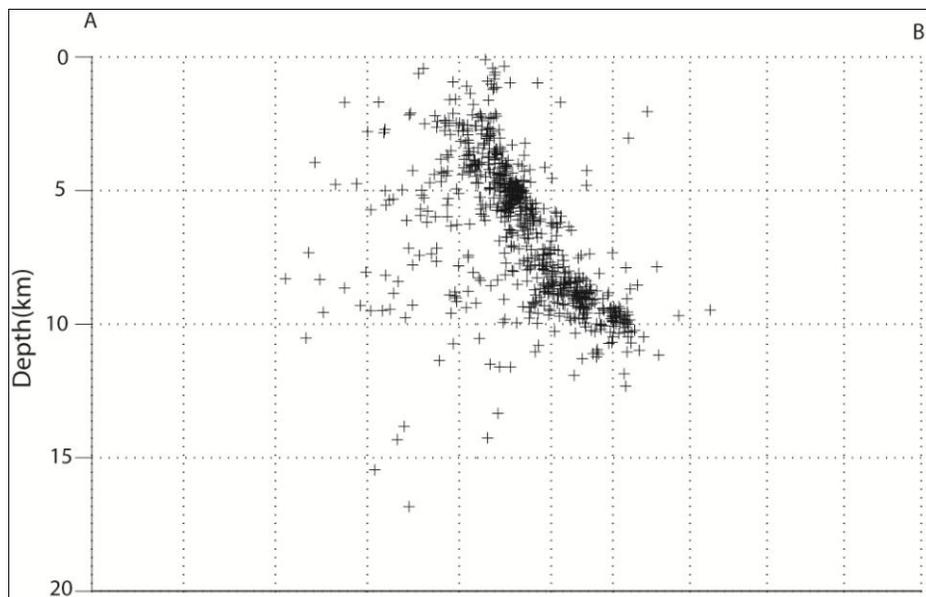
Figure 10. Cross-section view toward the N40E along the best alignment of aftershock data; aftershocks define a 55˚ SE-dipping fault plane. Reference is to the mean station elevation in the TCF basin, 1.82 km above sea level.
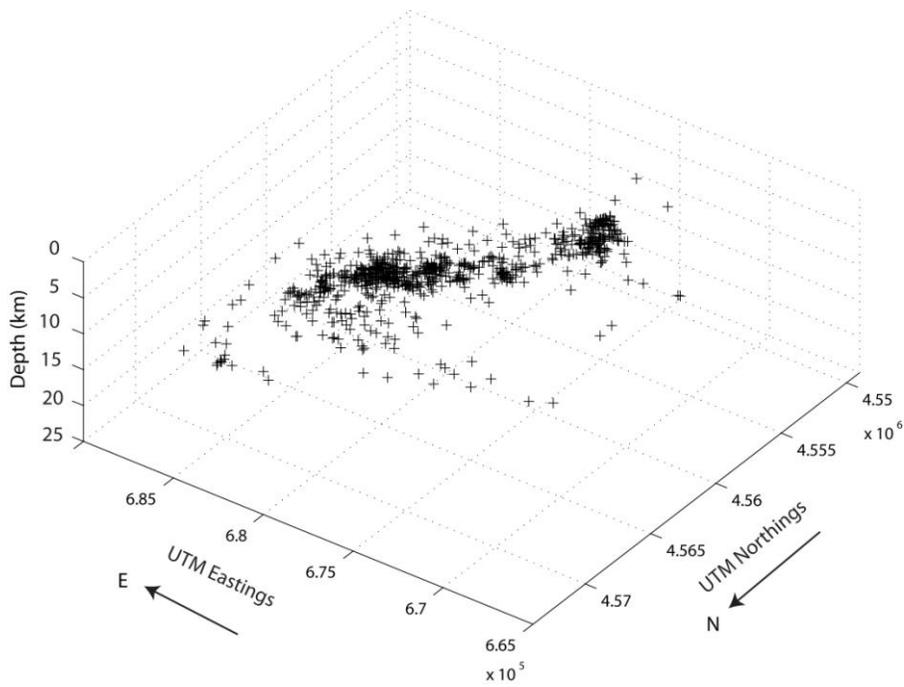
Figure 11. View from the NW down-dip, 55˚ SE, along the mainshock fault plane. The set of earthquakes at the SW edge (right) of the aftershock zone dips at about 42˚ SE (see figure 8).
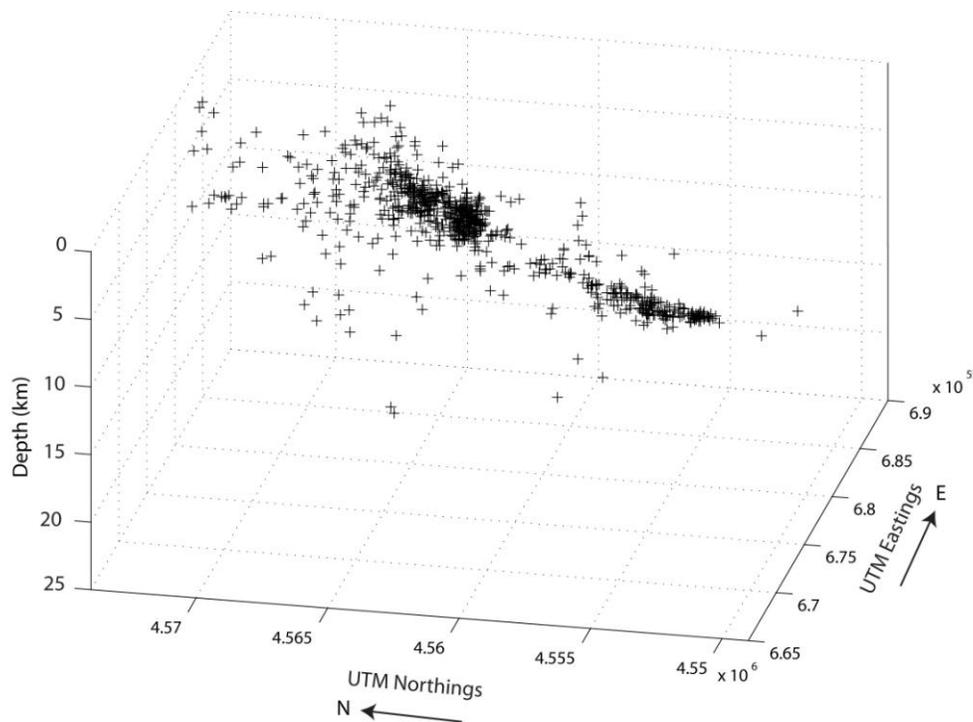
Figure 12. View from the WNW down-dip along the mainshock fault plane at 42˚ illustrating the shallow dip and alignment of earthquakes at the SW (right) extent of the aftershock zone. View is down the plunge of the white dashed structure shown in figure 9.
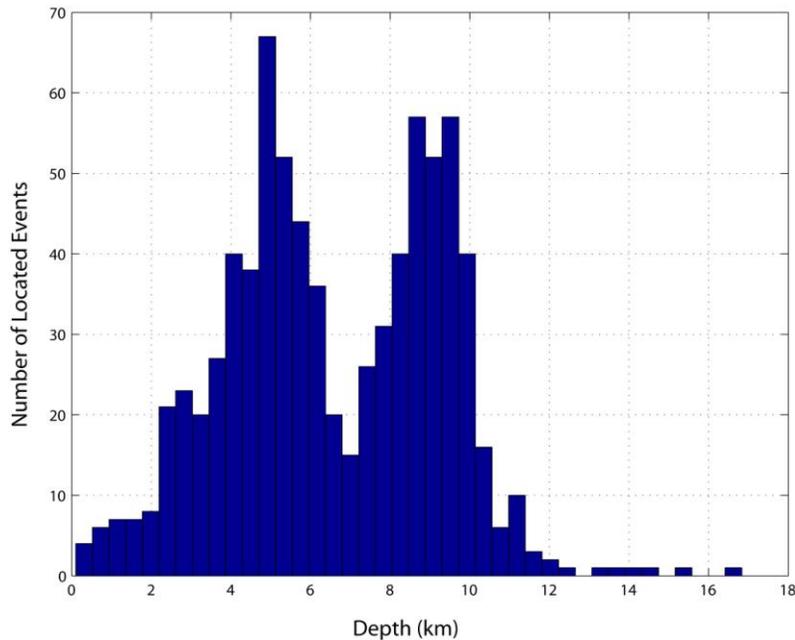
Figure 13. Histogram of relocated earthquake depths from portable instrument data period (highest quality locations). Reference is to the mean station elevation in the TCF basin, 1.82 km above sea level.

SPECULATION ON DEVELOPMENT OF TCF BASIN

The extent of faulting in the Wells earthquake and the aftershock distribution underlie a large portion of TCF basin. Bell (this volume) computes an InSAR image for the Wells event with a maximum deformation (nearly pure vertical) of about 15 cm centered on the mainshock location. The rupture extent from the InSAR image and other slip models (Dreger and others, 2008; Mendoza and others, 2008) is consistent with our interpretations of rupture from the aftershock distribution. Thus, the ratio of average displacement to subsidence is roughly 6 to 1. It is possible that TCF basin development has resulted from multiple Wells-type, or similar, earthquakes (non-surface faulting), where no single range-bounding fault has accommodated basin development. Estimating the basin elevation at about 250 meters below the Snake Mountains footwall block to the north, and an average estimated basin sediment thickness of 1750 meters (see Ponce and others, this volume for an estimated TCF basin depth of 2 km near the town of Wells based on gravity modeling, the deeper part of the basin) provides a basis for accounting for TCF deformation in Wells-type earthquakes. Simplistically assuming a 2 km offset between the Snake Range and the base of TCF, an average subsidence of 10 cm per Wells-type event (2/3 of the maximum InSAR determined subsidence) and ignoring erosion of the footwall block, about 20,000 Wells-type M_w 6.0 events would account for subsidence of the TCF basin relative to the Snake Mountains since roughly 9 Ma (i.e., estimated initiation of regional extensional deformation; see Henry and Colgan, this volume). Twenty-thousand events, based on these assumptions, would suggest a recurrence interval of 450 year for a M_w 6.0 Wells-type event. The mean subsidence rate of the basin since 9 Ma, accounting for a 2 km offset, is therefore about 0.2 mm/yr. These estimates are based on numerous assumptions and not intended to show defendable evidence for the evolution of TCF, but to provide insight into the development of similar minor basin structures in central Nevada. Down-to-the-north and down-to-the-west mapped Quaternary faults in Town Creek Flat basin (see Henry and Colgan, this volume) also play a role in TCF basin development. Despite the fact that no seismicity within the Wells sequence can be associated with these faults, they clearly contribute to deformation in TCF.

TCF should be considered a secondary structure associated with regional deformation that is driven by the major range-bounding faults, in particular the Ruby Mountains fault zone (RMFZ) east of Wells. The RMFZ has experienced M>7 earthquakes in the Quaternary. The total seismic moment in Wells-type events that account for a 2 km basin depth, within this set of assumptions, since 9 Ma is equivalent to 732 M_w 7.0 earthquakes (applying Hanks and Kanamori, 1992), resulting in a M_w 7.0 recurrence period of about 14 Ky (thousand years). Although poorly constrained, the slip rate for the RMFZ is estimated to be 0.2 mm/year, with a recurrence interval of less than 24 Ky and preferred return period of 10 Ka (from USGS Quaternary Fault Database; see references), consistent with this TCF deformation model. Therefore, TCF would experience roughly 20 M_w 6.0 events over a 10 Ka RMFZ return interval. These estimates provide generalizations about the development of minor basins within the context of overall regional deformation rates. Clearly, deformation

142

processes should not be assumed to have remained constant in eastern Nevada over 9 Ma (million years) and we have only attempted to estimate a recurrence interval for earthquakes, in basin development, that would be unlikely to have a surface expression. The question being, can small basins in Nevada develop without surface faulting events?

Ichinose and others (1998) identified structural transition zones, or slip transfer regions, connecting step-overs in Sierran range-bounding normal faults near the latitude of Reno, Nevada. Based on the rates of seismicity, they interpreted a Gutenburg-Richter recurrence behavior for the transition zones where the historical seismicity rates were high, and a characteristic recurrence for the major range-bounding structures that show little historical seismicity. In other words, the slip transfer regions show more frequent earthquakes, but at a lower maximum magnitude (based in part on the lack of through-going faulting) than the major range-bounding faults.

Clearly a small structure, the TCF basin can be considered a local accommodation feature associated with the Ruby Mountains-Snake Mountains-Clover Valley deformation zone. Nevertheless, these transition zones, or secondary structures, may play a role in the evolution of normal fault systems and regional tectonic processes that lead to large M_w 7+ normal faulting events. An implication of repeated moderate-sized earthquakes within small basins is that these depressions could form without experiencing surface faulting; TCF basin may reflect such a process. Although characterized by smaller earthquakes a shorter return period may imply a higher local seismic hazard.

SUMMARY AND CONCLUSIONS

The February 21, 2008 M_w 6.0 Wells earthquake involved normal faulting on an approximately N40°E-striking, 55° southeast-dipping fault plane in TCF basin northeast of Wells, Nevada. The locations of the mainshock and early aftershocks were constrained primarily by the EarthScope USArray Transportable Array that was fortunately operating in eastern Nevada at the time of the event. Near-source strong motion instrumentation was in place within hours of the event to capture on-scale near-source records of some of the largest normal faulting aftershocks (there is little near-source data for Basin and Range normal faulting events). HypoDD relocations of aftershocks using USArray and telemetered portable station data clearly define the orientation of the mainshock fault plane at depth. A N40°E strike direction is based on an interpretation of the dip and orientation of the aftershock locations within the central portion of the sequence. Aftershocks at the southwest end of the sequence suggest either a listric component of faulting or activity on an intersecting structure. An approximately 50 km^2 area free of aftershocks within the central mainshock fault plane is interpreted to roughly represent the extent of coseismic rupture. This estimate of the fault rupture area and the seismic moment of the event translate to a stress drop of approximately 89 bars and average displacement of 86 cm. Considering that no surface faulting has yet been identified for the Wells event and that the earthquake sequence involved most of TCF basin, we suggest that this small basin, and similar small basins in region, could be formed from repeated moderate-sized earthquakes without an expression of surface faulting.

Of particular value to an efficient and timely analysis of the Wells earthquake sequence was the implementation of an IP communications network to integrate real-time portable instrument data with regional network stations from various networks. This has eliminated traditional portable instrument data integration efforts, provided a set of phase arrivals and event locations in "one-pass" processing, improved remote portable network performance, enabled real-time access of near-source data to the community (through the IRIS DMC), and reduced overall operations costs. Integration and analysis of the wealth of portable instrument data collected during the Wells sequence are still under way. We greatly appreciate the enthusiastic cooperation and support of the community of Wells and public and private institutions in eastern Nevada, without which this study would not have been possible.

ACKNOWLEDGMENTS

REFERENCES

Bell, J.W., Caskey, S.J., Ramelli, A.R., Guerrieri, L., 2004, Pattern and rates of faulting in the central Nevada Seismic Belt, and paleoseismic evidence for prior beltlike behavior: Bulletin of the Seismological Society of America, v. 94, no. 4, p. 1229–1254.

Boore, D.M. and Joyner, W.B., 1997, Site amplifications for generic rock sites: Bulletin of the Seismological Society of America, v. 87, 327–341.

Busby, B., 2007, TA, *in* 2006 Annual Report, Incorporated Research Institutions for Seismology, Washington, D. C., 22–23.

Brune, J.N., 1970, Tectonic stress and the spectra of seismic shear waves from earthquakes: Journal of Geophysical Research. v. 75, p. 4997–5009.

Christenson, G.E., editor, 1995, The September 2, 1992, ML 5.8 St. George earthquake, Washington County, Utah: Utah Geological Survey Circular 88, 41 pp.

Clinton, J.F. and Heaton, T.H., 2002, Potential advantages of a strong-motion velocity meter over a strong-motion accelerometer: Seismological Research Letters, v. 73, p. 332–342.

Dreger, D.S., Ford, S.R., and Ryder, I., 2008, Finite source model of the February 21, 2008 M_w 6.0 Wells, Nevada earthquake [abs]: American Geophysical Union Fall Meeting, 2008, abstract #S51B-1743.

Henry, C.D., and Colgan, J.P., 2011, *this volume*, The regional structural setting of the Wells earthquake and Town Creek Flat basin–Implications for the Wells earthquake fault and adjacent structures.

Ichinose, G., Smith, K.D., and Anderson, J.G., 1997, Source Parameters of the 1995 Border Town, Nevada Earthquake Sequence: Bulletin of the Seismological Society of America, v. 87, p. 652–688.

Ichinose, G., Smith, K.D., and Anderson, J.G., 1998, Moment Tensor Solutions of the 1994 to 1996 Double Spring Flat, Nevada, Earthquake Sequence and Implications for Local Tectonic Models: Bulletin of the Seismological Society of America, v. 88, p. 1363–1378.

Mendoza, C., Hartzell, H., and Meremonte, M., 2008, Finite source study of the 2008 Wells, Nevada earthquake using regional broadband empirical Green's functions [abs]: American Geophysical Union Fall Meeting, 2008, abstract #S51B-1742.

Meremonte, M., Gomberg, G., and Cranswick, E., 1995, Constraints on the 29 June 1992 Little Skull Mountain, Nevada, earthquake sequence provided by robust hypocenter estimates: Bulletin of the Seismological Society of America, v. 85, p. 1039–1049.

Pechmann, J.C., Arabasz, W.J., and Nava, S.J., 1994, Refined analysis of the 1992 ML 5.8 St. George, Utah, earthquake and its aftershocks: Seismological Research Letters, v. 65, p. 32.

Pankow, K.L., Pechmann, J.C. and Arabasz, W.J., 2007, Use of ANSS strong-motion data to analyze small local earthquakes: Seismological Research Letters, v. 78, p. 369–374.

Pancha, P., Anderson, J.G., and Kreemer, C., 2006, Comparison of Seismic and Geodetic scale moment rates across the Basin and Range Province: Bulletin of the Seismological Society of America, v. 96, p. 11–32.

Peltzer, G., and Rosen, R., 1995, Surface displacement of the 17 May 1993 Eureka Valley, California earthquake observed by SAR Interferometry: Science, v. 268, p. 1333–1336.

Petersen, M.D., Frankel, A.D., Harmsen, S.C., Mueller, C.S., Haller, K.M., Wheeler, R.L., Wesson, R.L., Zeng, Y., Boyd, O.S., Perkins, D.M., Luco, N., Field, E.H., Wills, C.J., and Rukstales, K.S., 2008, Documentation for the 2008 update of the national seismic hazard maps: USGS Open File Report 2008-1128, 120 pp.

Ponce, D.A., Watt, J.T., and Bouligand, C., *this volume*, Geophysical setting of the February 21, 2008 M_w 6 Wells Earthquake, Nevada,–Implications for Earthquake Hazards.

Preistley, K.F., Smith K.D., and Cockerham, R.S., 1985, The 1984 Round Valley, California earthquake sequence, Geophysical Journal International, v. 95, issue 2, p. 215–235.

Rogers, A.M, Harmen, S.C., Corbett, E.J., Priestley, K.F., dePolo, D., 1991, The seismicity of Nevada and some adjacent parts of the Great Basin, *in* Slemmons, D.B., Engdahl, E.R., Zoback, M.D., and Blackwell, D.D., editors, Neotectonics of North America, Geological Society of America, Boulder, Colorado, Decade Map v. 1, p. 185–228.

Smith, K.D., Brune, J.N., Savage, M., dePolo, D.M., and Sheehan, A., 2001, The 1992 Little Skull Mountain earthquake sequence: Bulletin of the Seismological Society of America, v. 91, p. 1595–1606.

Smith, K.D. and Priestley, K.F., 2000, Faulting in the 1986 Chalfant, California, Sequence–Local Tectonics and Earthquake Source Parameters: Bulletin of the Seismological Society of America, v. 90, p. 813–831.

Smith, R.B. and Arabasz, W.J., 1991, Seismicity of the intermountain seismic belt, *in* Slemmons, D.B., Engdahl, E.R., Zoback, M.D., and Blackwell, D.D., editors, Neotectonics of North America, Geological Society of America, Boulder, Colorado, Decade Map v.1, p. 153–184.

U.S. Geological Survey, 2006, Quaternary fault and fold database for the United States, accessed November 2, 2008, from USGS web site: http//earthquakes.usgs.gov/regional/qfaults

Quinlan, D., 1995, Datascope: a relational database system for scientists; tutorial, version 1.1:
http://tagg.colorado.edu/software/tutorial/contents.html

Waldhauser, F. and Ellsworth, W.L., 2000, A double-difference earthquake location algorithm–method and application to the northern Hayward fault, California: Bulletin of the Seismological Society of America, v. 90, p. 1353–1368.

Wallace, R. E., 1984, Patterns and timing of Late Quaternary faulting in the Great Basin Province, and relation to some regional tectonic features: Journal of Geophysical Research, v. 89, p. 5763–5769.